MECSOL 2019 - Proceedings of the 7th International Symposium on Solid Mechanics
V. Tita, A. Ferreira, M.L. Ribeiro, A. Vieira and A.T. Beck (Editors), ABCM, Sao Carlos, SP, Brazil, April 15th to 17th, 2019

Computational prediction of a composite material response to impact by using a viscoelastic damage model

M. Urzedo Quirino[1], V. Tita[1] and M. L. Ribeiro[1]

[1] São Carlos School of Engineering, University of São Paulo — USP, Av. João Dagnone, 1100 - Jardim Santa Angelina, São Carlos, SP, Brazil - 13563-120.

Abstract: With the dissemination of composite materials in the aeronautical industry, including structural elements subject to impact loading, accurate damage models are becoming progressively necessary, in order to assess the material response to impact events and its capability of withstanding damage. This work proposes a damage model for composite materials, considering viscoelastic and temperature-dependent effects, inasmuch as many of the commonly employed composites have polymeric matrices; the model was, then, tested by comparison against experiment data.
Keywords: composite, impact, finite elements, viscoelasticity

INTRODUCTION

The use of composite materials in aeronautical industry is becoming progressively more generalized nowadays, bringing special interest in their properties under impact. This interest arises with the aim of designing structural elements with increased crashworthiness, improving safety, which, in turn, requires comprehension of the complex and diverse failure modes occurring simultaneously in the material (Ribeiro et al., 2013), in addition to requiring capacity of predicting impact damage size and its influence on the mechanical properties of the composite, especially on its residual strength (U. S. Department of Transportation, 2009).

Aiming for efficient and effective methodologies to predict impact damage, many authors (Ribeiro et al., 2013; Tan et al., 2015; Goldberg et al., 2018) have recently proposed constitutive damage models based on continuum mechanics, for use on finite element simulations. As many of the composites used on the aeronautical industry have polymeric matrices, viscoelastic behavior and temperature dependence are phenomena that have to be accounted for (Abouhamzeh et al., 2015); viscoelasticity also has a direct influence on elastic wave propagation inside the material (Prakash, 2012), and, consequently, on impact damage initiation processes.

Hence, the purpose of this work is to propose a damage model for composite materials under impact which also considers viscoelastic and temperature-dependent effects from the matrix. This damage model was tested with an impact simulation, by computationally modeling the assembly present in Ribeiro et al., 2013, and, subsequently, comparing the experimental results from that research with those obtained from the simulations. Furthermore, this work presents comparisons considering the overall influence of viscoelasticity and temperature on the results, and the influence of the model boundary conditions on the latter.

MATERIAL MODEL

The composite was considered as a plane-stress viscoelastic material allowing fiber and matrix damage, properly written as a VUMAT (Vectorized User Material) subroutine, for simulation with the commercial finite element software ABAQUS™; the constitutive model employed on the simulations is presented below.

Viscoelastic behavior

Stress relaxation effects were considered by adopting the model proposed by Abouhamzeh et al., 2015: linear viscoelastic behavior is accounted for by modeling the material as a set of linear Maxwell networks in parallel, each with its own stiffness and relaxation time, as of Fig. 1.

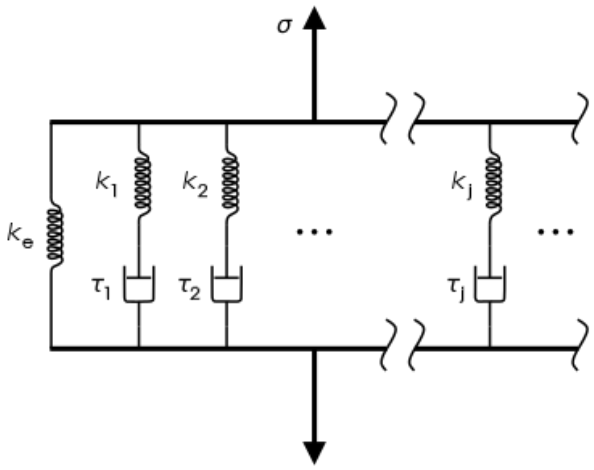

Figure 1 – Generalized Maxwell rheological model, Pekaje, 2007

Each component of the material stiffness tensor is calculated from Eq. 1 below, as of Abouhamzeh et al., 2015, with C_{ij} being the material stiffness tensor components at time t, with the influence of temperature explicited and explained at the following section. The tensor was written as a Prony series expansion, with the term C_{ij}^{∞} being the fully relaxed stiffness components, and C_{ij}^{m} the transient ones, subjected to exponential decays with independent time constants, τ_{ij}^{m}, for each stiffness component and for each of the N_m Maxwell networks; this work considers the composite as a single Maxwell network, however. Nevertheless, material behavior at the fiber-dominated direction was considered as linear elastic, thus independent of time and temperature.

$$C_{ij}(t) = C_{ij}^{\infty} + \sum_{m=1}^{N_m} C_{ij}^{m} \exp\left(-\frac{t}{\tau_{ij}^{m}}\right) \tag{1}$$

The fully relaxed and the transient stiffness tensors were considered functions of the elastic properties from Ribeiro et al., 2013, by properly multiplying the elastic stiffness tensor, $C_{ij}^{elastic}$, by a stiffness relaxation factor, R, as of Eqs. 2 and 3, below:

$$C_{ij}^{\infty} = RC_{ij}^{elastic} \tag{2}$$

$$C_{ij}^{m} = (1-R)C_{ij}^{elastic} \tag{3}$$

With both stiffness tensors, the stresses were determined according to the analytic incremental solution, Eq. 4, adapted from Abouhamzeh et al., 2015, which relates the current stress components, $\sigma_i(t_n)$ to those from the previous time increment, $\sigma_i(t_{n-1})$; the model is presented below, already simplified to the single network case.

$$\sigma_i(t_n) = \sigma_i(t_{n-1}) + C_{ij}^{elastic}\left\{R + (1-R)\frac{\tau_{ij}}{\Delta t}\left[1-\exp\left(-\frac{\Delta t}{\tau_{ij}}\right)\right]\right\}\Delta\varepsilon_i + \left[\exp\left(-\frac{\Delta t}{\tau_{ij}}\right) - 1\right] S_{ij}(t_n) \tag{4}$$

Above, $\Delta\varepsilon_i$ are the strain increment components, with Δt being the simulation step time increment, whereas $S_{ij}(t_n)$ are the stress components acting on the network, recursively calculated from their previous values, $S_{ij}(t_{n-1})$, according to Eq. 5, also adapted from Abouhamzeh et al., 2015.

$$S_{ij}(t_n) = \exp\left(-\frac{\Delta t}{\tau_{ij}}\right) S_{ij}(t_{n-1}) + \frac{\tau_{ij}}{\Delta t}(1-R)C_{ij}^{elastic}\left[1-\exp\left(-\frac{\Delta t}{\tau_{ij}}\right)\right]\Delta\varepsilon_j \tag{5}$$

Damage model

According to Herakovich, 1998, it was experimentally verified that only fiber breakage degrades the fibrous composite longitudinal (fiber-dominated direction) modulus; therefore, fiber damage and matrix damage were evaluated separately.

Fiber damage

Modeling of fiber damage was done according to Ribeiro, 2013, associating failure at the fiber-dominated direction with a corresponding degradation of the material longitudinal modulus; fiber failure was considered as entirely governed by the longitudinal normal stress (σ_{11}).

1. Fiber damage under longitudinal tension

   The maximum stress criterion, shown on Eq. 6, was used to model fiber tensile damage:

$$FF_T = \left(\frac{\sigma_{11}}{X_T}\right)^2 \tag{6}$$

   Above, X_T represents the material longitudinal tensile strength, FF_T being the failure parameter: complete tensile fiber failure occurs if this parameter becomes greater than unity, bringing the longitudinal modulus, E_{11}, and Poisson's ratio ν_{21} down to 1% of their proper undamaged values.

2. Fiber damage under longitudinal compression

   Fiber damage under compression is also modeled through the maximum stress criterion, as of Eq. 7:

$$FF_C = \left(\frac{\sigma_{11}}{X_C}\right)^2 \tag{7}$$

   X_C represents the material longitudinal compressive strength, with FF_C being the parameter for gradual failure: when its value becomes greater than unity, it triggers a progressive degradation of the longitudinal modulus and Poisson's ratio ν_{21}, due to nonlinear geometric effects related to ply behavior; these nonlinear effects were modeled through a polynomial fit of experiment data (extracted from Ribeiro, 2013).

Matrix damage

Matrix damage was evaluated according to the model presented by Ribeiro, Tita, and Vandepitte, 2012, which proposes progressive degradation of the properties at the transverse (matrix-dominated) direction, with the onset of failure triggered by the transverse normal stress (σ_{22}) and the inplane shear stress (σ_{12}) only, independently of the longitudinal normal stress. Degradation is considered irreversible, measured with monotonically-increasing damage variables, whose evolution occurs only when the failure initiation criterion of Eq. 8 is met.

1. Damage initiation

   The initiation law for matrix damage is expressed by Eq. 8, f being the failure variable, and S_{12_y} and σ_{22_0} being experimentally determined constants, whose values were extracted from Ribeiro, 2013.

$$f = \sqrt{\sigma_{22}^2 + \sigma_{12}^2} - S_{12_y}\left[-1 + \frac{2}{1 + \left(\frac{|\sigma_{22}|}{\sigma_{22_0}}\right)^3}\right] \tag{8}$$

2. Matrix shear damage

   Once damage is initiated (f being greater than zero), the shear damage variable, d_6, is calculated from its respective thermodynamic force, Y_6: the latter is calculated first, from the current stress state and the previous value of its corresponding damage variable, as expressed by Eq. 9, whereas the former is, then, updated, considering the fiber orientation angle, θ, of each layer, as of Eq. 10. The composite shear modulus is, then, progressively degraded, by a factor of $(1 - d_6)$.

$$Y_6 = \sqrt{\frac{\sigma_{12}^2}{2G_{12}\left(1-d_6\right)^2}} \tag{9}$$

$$d_6 = (C\theta + D)Y_6 - Y_{6_0} \tag{10}$$

Above, G_{12} is the undamaged shear modulus, with C and D being experimentally determined constants (from Ribeiro, 2013), and Y_{6_0} being the first value of the shear thermodynamic force, calculated when damage initiation first occurs. Complete shear failure occurs when d_6 reaches its upper limit of 0.99, reducing the material shear modulus to 1% of its undamaged value.

3. Matrix damage under transverse tension

As the shear damage case, the damage variable for transverse normal stress, d_2, and its corresponding thermodynamic force, Y_2, were defined in an analogous manner, as of eqs. 11 and 12, below, with E_{22} being the undamaged transverse modulus, A and B being experimentally determined constants (from Ribeiro, 2013), and Y_{2_0} being the thermodynamic force for transverse normal stresses when damage initiation first occurs. As in the shear damage case, Y_2 is evaluated with the previous value of d_2, which is, then, updated.

$$Y_2 = \sqrt{\frac{\sigma_{22}^2}{2E_{22}\left(1-d_2\right)^2}} \tag{11}$$

$$d_2 = (A\theta + B)Y_2 - Y_{2_0} \tag{12}$$

Degradation of the tranverse modulus and Poisson's ratio ν_{21}, thus, occurs through a factor of $(1-d_2)$, with complete failure taking place when d_2 reaches its upper limit of 0.99, bringing both material properties down to 1% of their respective undamaged values.

4. Matrix damage under transverse compression

From Ribeiro, Tita and Vandepitte, 2012, matrix damage under transverse compression was evaluated considering nonlinear geometric behavior: failure initiation (Eq. 8) triggers progressive degradation of the transverse modulus and Poisson's ratio ν_{12}, modeled through a polynomial fit of experiment data (from Ribeiro, 2013), similarly to the evaluation of fiber damage under compression. Nevertheless, for cases in which the normal transverse strain is tensile, even though the transverse normal stress is compressive, damage is, instead, calculated through the thermodynamic force approach, using eqs. 11 and 12, with values of parameters A and B taken from experiments (from Ribeiro, 2013) considering compression.

Complete failure brings both the transverse modulus and Poisson's ratio ν_{12} down to 1% of their respective undamaged values. In this case, it may happen because of nonlinear geometric effects (transverse compressive strain) or due to the damage variable d_2 reaching its upper limit of 0.99.

5. Strain energy failure

Complete matrix failure is also allowed to occur whenever the specific strain energy associated to the current stress state reaches the experimentally determined (Ribeiro, 2013) material limit; if this occurs, both matrix damage variables, d_2 and d_6, become immediately their upper limits, bringing all the three matrix-dominated properties (E_{22}, ν_{21}, G_{12}) down to 1% of their respective undamaged values. Evaluation of the specific strain energy, U, is done as of Eq. 13, with ε_{22} being the transverse normal strain, and γ_{12} being the inplane engineering shear strain.

$$U = \frac{1}{2}\left(|\sigma_{22}\varepsilon_{22}| + |\sigma_{12}\gamma_{12}|\right) \tag{13}$$

MATERIAL PROPERTIES

The modeled composite was a cross-ply carbon–epoxy prepreg M10, with layup $[0°/90°/0°/90°/0°]_S$; its elastic properties and values of strength, considering plane stress, were obtained from simulations coupled with experimental tests (as of Ribeiro et al., 2013). The values of the material properties are listed under Tab. 1, and Tab. 2, below:

Table 1 – Elastic properties and mass density of the composite material

Elastic properties	Values
E_{11} (longitudinal elastic modulus) [GPa]	127.0
E_{22} (transverse elastic modulus) [GPa]	10.00
ν_{12} (Poisson's ratio)	0.34
G_{12} (shear modulus) [GPa]	5.40
ρ (mass density) [kg/m^3]	1 580

Table 2 – Values of strength for the composite material

Strengths	Values
X_T (longitudinal tensile strength) [MPa]	1 400
X_C (longitudinal compressive strength) [MPa]	930.0

For its temperature-dependent viscoelastic properties, the composite creep master curve was extracted from Goertzen and Kessler, 2006, with the relaxation modulus obtained from it, through Eqs. 14 and 15, from Park and Kim, 1999. Below, $G(t)$ represents the relaxation modulus, and $J(t)$ the creep compliance.

$$G(t) = \frac{1}{J(t)} \frac{\sin(n\pi)}{n\pi} \tag{14}$$

$$n = \left| \frac{d\{\log[J(t)]\}}{d\{\log(t)\}} \right| \tag{15}$$

Tem The creep compliance master curve from which the relaxation modulus was extracted corresponded to a reference temperature of 30°C. In order to assess the effects of temperature changes on the simulation results, time-temperature shifts were performed on the relaxation curve, through the shift factor a_T, as of Eq. 16, with t' being the reduced timescele and t_0 the unshifted timescale.

$$t' = \frac{t_0}{a_T} \tag{16}$$

Calculation of the shift factor was performed as of Arrhenius relationship, Eq. 17, from Goertzen and Kessler, 2006, with ΔH being the molar activation energy, whose value was taken from said reference; $\overline{R}$ represents the universal gas constant, T the current temperature, and T_{ref} the reference temperature.

$$\ln(a_T) = \frac{\Delta H}{\overline{R}} \left(\frac{1}{T} - \frac{1}{T_{ref}} \right) \tag{17}$$

Properly shifted, the data were extrapolated to shorter timescales and fitted to Prony series, as of Eq. 1, although with a single exponential term. From the data fits, the relaxation times were obtained, being considered the same for transverse and shear moduli, and for Poisson's ratio, but assumed extremely large for the longitudinal modulus; also, the stiffness relaxation factors, R, were estimated by dividing the value of the series at zero time by its value at infinite time. The results are shown under Tab. 3, below, for temperatures of 30°C (unshifted), 20°C and 10°C, the latter being the average temperature at which the results from Ribeiro et al., 2013 were obtained.

Table 3 – Viscoelastic properties for the composite material, at different temperatures

Viscoelastic properties			
T (current temperature) [°C]	10.0	20.0	30.0
ΔH (molar activation energy) [kJ/mol]	324.0		
T_{ref} (reference temperature) [°C]	30.0		
$\overline{R}$ (gas constant) [J/kg·K]	8.314		
a_T (time shift factor)	8 778.9	80.25	0.0
R (stiffness relaxation factor)	0.4823	0.5509	0.5444
τ_{11} (relaxation time for longitudinal modulus) [s]	Assumed infinite		
τ_{22} (relaxation time for transverse modulus) [s]	$4.618{\cdot}10^9$	$4.222{\cdot}10^7$	$5.260{\cdot}10^5$
τ_{12} (relaxation time for Poisson's ratio) [s]	$4.618{\cdot}10^9$	$4.222{\cdot}10^7$	$5.260{\cdot}10^5$
τ_{12} (relaxation time for shear modulus) [s]	$4.618{\cdot}10^9$	$4.222{\cdot}10^7$	$5.260{\cdot}10^5$

FINITE ELEMENT MODEL

The low-velocity impact test on the composite plate was simulated on ABAQUS^{TM}, with explicit steps and automatic time increments, employing a subroutine VUMAT for the material model. The plate was modeled with linear full-integration shell elements, with 3 integration points through each layer thickness; realistic boundary conditions were simulated by clamping the plate between two steel disks, modeled with solid full-integration hexaedron elements. One of the disks had all its degrees of freedom restrained, whereas the other was attached to the first one through four screws, modeled with solid reduced-integration hexaedron elements; a torque of 27 N.m was simulated on the screws, by applying a 0.157 mm displacement on the free disk.

For modeling contact between the composite and the disks and between the former and the impactor, a hard contact algorithm was imposed at the normal direction, and a penalty contact algorithm with a friction coefficient of 0.1 was imposed at the tangent direction; the impactor was modeled with rigid quadrilateral elements, with a total mass of 1.2 kg concentrated at its reference point, and an initial velocity of 3.13 m/s. The finite element model is presented under Fig. 2, below.

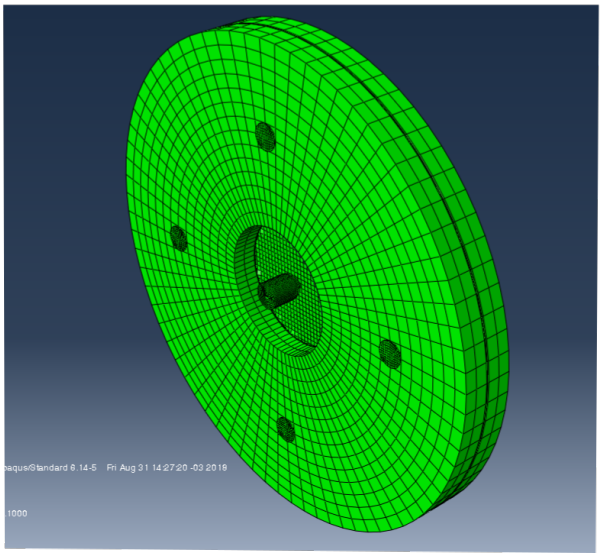

Figure 2 – Finite element model

RESULTS

Influence of viscoelasticity and temperature

In order to evaluate the effectiveness of the damage model and the influence of viscoelasticity on the material behavior, four cases were simulated: one purely elastic and three viscoelastic; both cases were, thus, compared with experimental results from Ribeiro et al., 2013. The results are shown below, on Fig. 3, with relevant parameters for comparison between results also shown under Tab. 4.

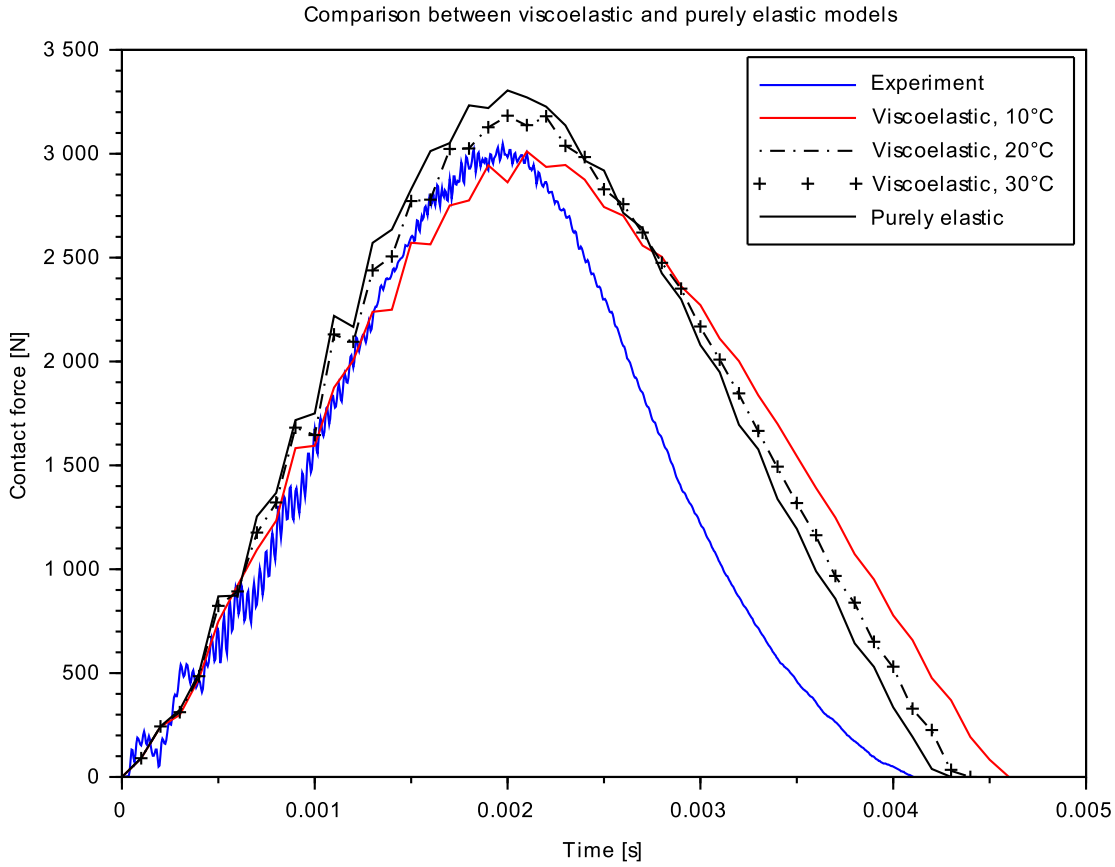

Figure 3 – Contact force history for experimental, elastic and viscoelastic cases

Table 4 – Comparison of experiment and simulation results - effect of viscoelasticity

Cases	Experiment	Viscoelastic, 10°C	Viscoelastic, 20°C	Viscoelastic, 30°C	Elastic
Impact duration [ms]	4.095	4.600	4.400	4.400	4.300
Peak normal contact force [N]	3 048	3 011	3 182	3 183	3 305
Peak force instant [ms]	1.975	2.1000	2.000	2.000	2.000

The viscoelastic cases at 20°C and 30°C present very similar responses between each other, as their respective curves are practically coincident; on the other hand, the viscoelastic case at 10°C presents the closest estimation of the peak normal contact force, with a difference of less than 2.0%, in comparison to 4.4% for the other temperatures and 8.4% for the purely elastic case. Nevertheless, the 10°C case presents the largest difference of impact duration, in comparison to the experimental case, being of 12.3%, in contrast to that of the elastic case (5.0%); in addition, the 10°C case showed the

largest difference in peak force instant from the experimental case (6.3%), in comparison to the other cases (1.2%).

Influence of boundary conditions

The sensitivity of the model to changes in boundary conditions was evaluated through comparison of results, considering different values of contact friction and torque on the fixation screws.

Friction coefficient

Results for different values of the friction coefficient, applied and modified at all contact surfaces in the model, were assessed, being presented on Fig. 4 and on Tab. 5, below.

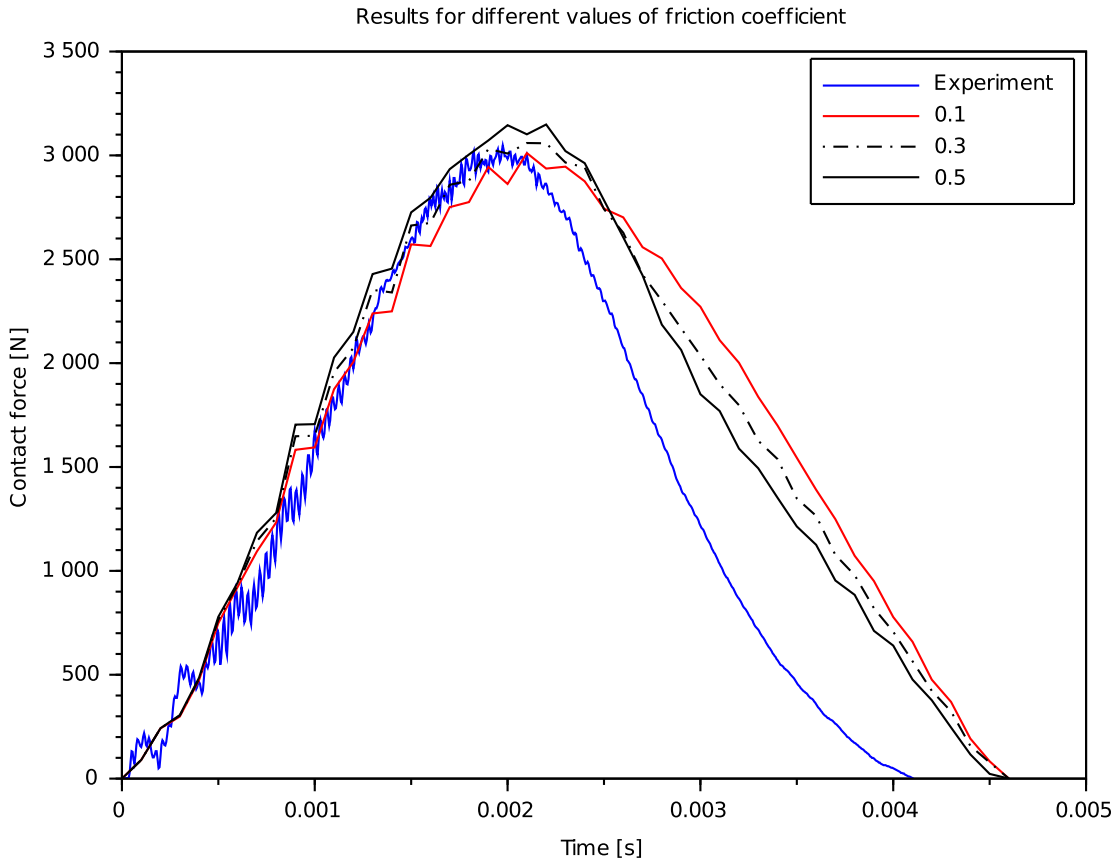

Figure 4 – Contact force history, for different values of contact friction

Table 5 – Comparison of experiment and simulation results - effect of contact friction

Friction cases	Experiment	0.1	0.3	0.5
Impact duration [ms]	4.095	4.600	4.600	4.600
Peak normal contact force [N]	3 048	3 011	3 060	3 149
Peak force instant [ms]	1.975	2.100	2.100	2.200

From above, changes of the friction coefficient are shown to have negligible effect on impact duration. For increasing values of the friction coefficient, the peak force instants suffered only slight shifts to later times, while the normal contact

forces increased, although by an amount no greater than 5.0%, in relation to the case with the lowest friction coefficient.

Torque on the screws

The model sensitivity to different values of torque on the four fixation screws was evaluated and presented below, on Fig. 5; different torque values were modeled by applying different displacements on the four screws: torques of 27 N·m, 50 N·m, and 100 N·m were modeled as displacements of 0.157 mm, 0.291 mm, and 0.582 mm, respectively.

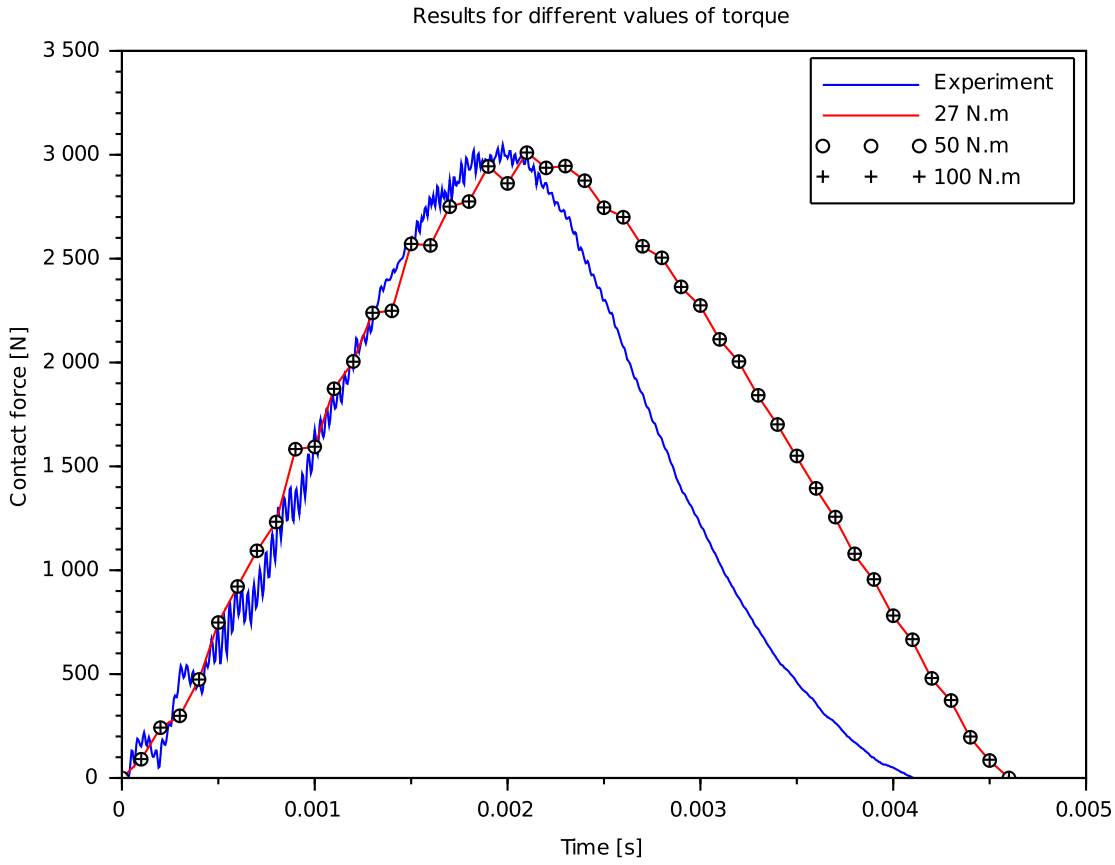

Figure 5 – Contact force history, for different values of fixation screw torque

Inasmuch as the three simulation curves above are practically coincident, the computational results are shown to be not sensitive to changes in the fixation screws torque.

CONCLUSIONS

This work presented a damage model for composite materials, considering their viscoelastic and temperature-dependent behavior. The damage predictions through the force history showed relatively good agreement, although the impact duration and, consequently, the energy absorbed were, in many of the cases,found to be higher, showing, thus, the necessity of improvements, such as evaluation of plastic behavior. Nevertheless, simulations with the material at 10°C (approximately the same from the experimental data), even with considerable differences in impact duration and peak force instant, predicted well the peak normal contact force. In addition, whereas the model showed to be insensitive to changes in the torque of fixation screws, adding friction tended to move the results towards the purely elastic case.

REFERENCES

Abouhamzeh, M., Sinke, J., Jansen, K. M. B., Benedictus, R., 2015, "A new procedure for thermo-viscoelastic modelling of composites with general orthotropy and geometry", Composite Structures, Vol.133, pp. 871-877, http://dx.doi.org/10.1016/j.compstruct.2015.08.050.

Goertzen, W. K., Kessler, M. R., 2006, "Creep behavior of carbon fiber/epoxy matrix composites", Materials Science and Engineering, Vol.A 421, pp. 217-225, https://doi.org/10.1016/j.msea.2006.01.063

Goldberg, R. K., Carney, K. S., DuBois, P., Hoffarth, C., Khaled, B., Rajan, S., Blankenhorn, G., 2018, "Analysis and characterization of damage using a generalized composite material model suitable for impact problems", Journal of Aerospace Engineering, Vol.31, No. 4, 10 p. https://doi.org/10.1061/(ASCE)AS.1943-5525.0000854.

Herakovich, C. T., 1998, "Mechanics of Fibrous Composites", Ed. John Wiley & Sons, Inc., New York, ch. 9, pp. 303-362.

Park, S. W., Kim, Y. R., 1999, "Interconversion between relaxation modulus and creep compliance for viscoelastic solids", Journal of Materials in Civil Engineering, Vol.11, No. 1, pp. 76-82. https://doi.org/10.1061/(ASCE)0899-1561(1999)11:1(76)

Pekaje, 2007, "Generalized Maxwell Model: Maxwell–Weichert model for viscoelastic materials", original height: 2000 pixels, original width: 1500 pixels, original size: 63,9 Kb, PNG, https://commons.wikimedia.org/wiki/File:Composite_laminate_ specimen.JPG.

Prakash, V., 2012, "Shock and Impact Response of Glass Fiber-Reinforced Polymer Composites", in: Thomas, S., Joseph, K., Malhotra, S. K., Goda, K., Sreekala, M. S. (Eds.), Polymer Composites: Volume 1, Ed. Wiley-VCH Verlag & Co. KGaA, Weinheim, Germany, ch. 2, pp. 17-82.

Ribeiro, M. L., Tita, V., Vandepitte, D., 2012, "A new damage model for composite laminates", Composite Structures, Vol.94, pp. 635-642, http://dx.doi.org/10.1016/j.compstruct.2011.08.031

Ribeiro, M. L., 2013, "Damage and progressive failure analysis for aeronautic composite structures with curvature", Doctoral thesis, 236 p., São Carlos School of Engineering, University of São Paulo, São Carlos, Brazil, Faculty of Engineering Science, Catholic University of Leuven, Leuven, Belgium, http://www.teses.usp.br/teses/disponiveis/18/.../tde.../MarceloLeiteRibeiroDO.pdf.

Ribeiro, M. L., Angélico, R. A., Medeiros, R., Tita, V., 2013, "Finite element analyses of low velocity impact on thin composite disks", International Journal of Composite Materials, Vol.3(6B), pp. 59-70, http://article.sapub.org/10.5923.s.cmaterials.201310.07.html.

Tan, W., Falzon, B. G., Chiu, L. N. S., Price, M., 2015, "Predicting low-velocity impact damage and compression-after-impact (CAI) behaviour of composite laminates", Composites: Part A, Vol.71, pp. 212-226, http://dx.doi.org/10.1016/j.compositesa.2015.01.025

U. S. Department of Transportation, 2009, "Federal Aviation Administration. Advisory Circular 20-107B with change 1: Composite Aircraft Structure", 38 p. https://www.faa.gov/documentLibrary/media/Advisory_Circular/AC_20-107B_with_change_1.pdf..

RESPONSIBILITY NOTICE

The authors are the only responsible for the printed material included in this paper.